The structure of rare earth thin films: holmium and gadolinium on yttrium

2003 J. Phys.: Condens. Matter 15 7155

(http://iopscience.iop.org/0953-8984/15/43/002)

INSTITUTE OF PHYSICS PUBLISHING JOURNAL OF PHYSICS: CONDENSED MATTER

J. Phys.: Condens. Matter **15** (2003) 7155–7174 PII: S0953-8984(03)62963-2

The structure of rare earth thin films: holmium and gadolinium on yttrium

M J Bentall[1,3], R A Cowley[1], R C C Ward[1], M R Wells[1] and A Stunault[2,4]

[1] Oxford Physics, Clarendon Laboratory, Parks Road, Oxford OX1 3PU, UK
[2] XMaS, The European Synchrotron Radiation Facility, BP 220, 38043 Grenoble Cedex, France

E-mail: m.bentall1@physics.ox.ac.uk

Received 28 April 2003
Published 17 October 2003
Online at stacks.iop.org/JPhysCM/15/7155

Abstract

Single-crystal holmium and gadolinium layers have been grown on yttrium substrates using the molecular beam epitaxy technique and their structures investigated using high resolution x-ray scattering. The experiments were performed using a Philips MRD diffractometer in Oxford, and with the XMaS facility at the ESRF. Holmium layers with a thickness below $T_c' = 115$ Å give scattering that is characteristic of a pseudomorphic film structure with the same in-plane lattice parameter as the yttrium substrate to within 0.05%. For layers thicker than T_c', there is a sharp reduction in misfit strain due to the creation of edge dislocations. The transverse lineshape of the holmium peaks exhibits a two-component lineshape for thicknesses above T_c', but below about 500 Å. Above 500 Å the lineshape of the transverse scans becomes Gaussian and is characteristic of a mosaic crystal.

The gadolinium layers show no sharp change of strain for layers as thick as 2920 Å and the transverse peak shape remained similar for all films. This is characteristic of pseudomorphic film growth and a failure to nucleate dislocations.

(Some figures in this article are in colour only in the electronic version)

1. Introduction

The ability to predict the conditions needed for the growth of high quality pseudomorphic thin layers is important for thin film research and particularly vital for semiconductor systems that are used to create solid state devices. If the structure is strained the optical and transport properties are adversely affected by the dislocations relieving the strain.

It is generally agreed that below a critical thickness an epitaxial layer can grow coherently strained on a substrate, so that the resulting in-plane lattice parameter of the layer is lattice

[3] Author to whom any correspondence should be addressed.
[4] Present address: Institut Laue Langevin, 6 rue Jules Horowitz, BP 156, F-38042 Grenoble Cedex 9, France.

matched to that of the substrate. This is known as a pseudomorphic film. Above the critical thickness, dislocations are introduced and the lattice parameter of the layer tends towards that of the bulk.

We have studied holmium and gadolinium layers grown on sapphire substrates with niobium buffer and yttrium seed layers. This is the route used to grow rare earth layers and superlattices, largely for their magnetic properties, and we are unaware of any previous work concerning the change in their structure with thickness.

Niobium and sapphire have a large lattice mismatch, so the critical thickness before the introduction of dislocations is only a few monolayers. The simplest theory for the estimation of the critical thickness, T_c, is essentially a two-dimensional (2D) model where dislocations are introduced when the homogeneous strain energy of the layer exceeds the dislocation formation energy. This theory is equivalent to the Matthews and Blakeslee theory [1]. Using this theory with a modification by Downes [2] for intermediate strains gives the critical thickness of niobium on sapphire as about 70 Å. The structure of niobium layers on sapphire has been well studied [3–6]. For layers with a thickness of less than 1000 Å, the scattering has a characteristic two-component lineshape for the transverse scans. There is a sharp resolution-limited peak that arises because the niobium planes are, on average, flat over distances of 50 000 Å. This is accompanied by much broader diffuse scattering from the dislocations that follows a $1/q_x^3$ behaviour. The presence of the dislocations has been confirmed by the use of high resolution electron microscopy (HREM) [5] and shows that there are two possible dislocation networks. For a 190 Å layer of niobium on sapphire, Barabash *et al* [6] have shown it to contain 95% edge dislocations with Burgers vectors $\boldsymbol{b} = 1/3[\bar{1}12]$ and $\boldsymbol{b} = 1/2[1\bar{1}1]$, creating an orthogonal array of dislocations with Burgers vectors in the (110) growth plane. There are also a minority (5%) of dislocations with Burgers vectors $\boldsymbol{b} = 1/2[1\bar{1}1]$ and $\boldsymbol{b} = 1/2[\bar{1}11]$, which create a non-orthogonal array of dislocations.

Yttrium layers grown on a niobium buffer show a similar form of x-ray scattering to that of the niobium buffer [7].

Unfortunately, rare earth layers grown on yttrium have not yet been studied using high resolution transmission electron microscopy (HRTEM) or conventional transmission electron microscopy (TEM). However, measurements have been made using HRTEM on holmium–yttrium superlattices [8]. These measurements have shown the existence of misfit dislocations at the holmium–yttrium interfaces with a Burgers vector $\boldsymbol{b} = 1/3\langle 11\bar{2}0\rangle$ in the (0001) growth plane. TEM and resolved shear stress measurements have also been made on the bulk elements and these measurements have shown that the likely slip systems are $\langle 11\bar{2}0\rangle\{0001\}$ and $\langle 11\bar{2}3\rangle\{11\bar{2}2\}$ with a Burgers vector $\boldsymbol{b} = 1/3\langle 11\bar{2}0\rangle$ and $1/3\langle 11\bar{2}3\rangle$, respectively [9], in agreement with the thin layer work on holmium–yttrium superlattices.

In this study we have used high resolution x-ray diffraction techniques to study the x-ray scattering around several Bragg reflections of holmium and gadolinium layers grown on yttrium.

In section 2 we detail the experimental method, while section 3.1 describes the results obtained for holmium layers and we show that there is a critical thickness of $T_c' = 115$ Å for the onset of misfit dislocations. This is ten times larger than the critical thickness obtained theoretically. Section 3.2 reports similar results for gadolinium layers. Although theory gives $T_c' = 300$ Å, we find no evidence for substantial lattice parameter relaxation below 3000 Å. The results are discussed and summarized in the final section.

2. Experiments

A series of seven different samples of thin layers were grown using the Balzers molecular beam epitaxy facility at Oxford. The substrate was $(11\bar{2}0)$ sapphire on which a niobium buffer layer

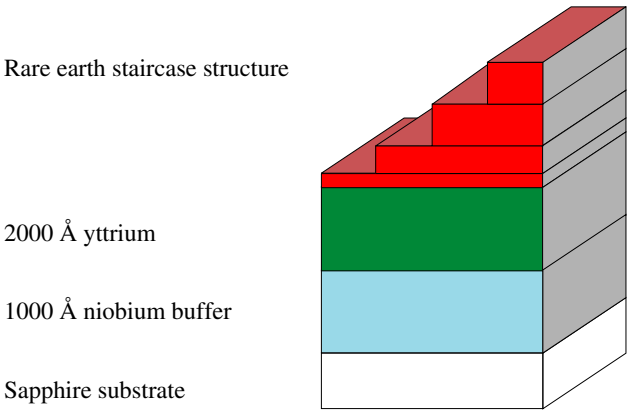

Figure 1. A schematic diagram of the more complex terrace structure samples used in this study.

of 1000 Å thickness and [110] growth direction was grown at 800 °C. A 2000 Å thick seed of yttrium was deposited at 550 °C and the temperature was reduced to 350 °C over the course of the deposition. The (0001) planes were perpendicular to the growth axis. This was followed by the deposition of a terrace, figure 1, or thin layer structure of holmium or gadolinium at 350 °C and the structure was sealed with a 50 Å niobium cap to prevent oxidation of the rare earth layer.

The growth process was monitored *in situ* using RHEED diffraction and the patterns exhibited streaks with maxima at the 2D positions, showing that the layers grew in a two-dimensional mode. However, the growth was not layer by layer because there were no RHEED oscillations and the surface had a steady-state roughness which was estimated at 3–4 atomic planes.

Niobium, yttrium and gadolinium were evaporated using electron beam sources, while holmium was evaporated in a conventional K-cell. The thickness was controlled by calibrating the elemental fluxes immediately before the sample growth using a quartz crystal monitor located exactly at the substrate position. Control systems maintained stable fluxes throughout the growth, allowing the thickness of the layer to be determined by the growth time. This estimate of the layer thickness is referred to as the nominal thickness. The simpler samples consisted of a rare earth thin layer of uniform thickness. In order to simplify the x-ray diffraction experiments, and to maintain as uniform growth conditions as possible for the different layers, in some cases a novel terrace structure was grown by progressively moving a linear shutter through the flux of atoms, as schematically illustrated in figure 1.

2.1. X-ray scattering

The structures of the layers were investigated with x-ray scattering techniques using the XMaS beamline (BM28) at the ESRF with an incident energy of 11 keV and a wavelength of 1.127 Å. The diffractometer was used in a triple-axis mode, with a Ge(111) analyser crystal. For the experiments performed in Oxford, a triple-crystal Philips MRD high resolution x-ray diffractometer was used with an incident wavelength of 1.540 56 Å from a copper target. The scattering vector, $\boldsymbol{Q}$, was varied parallel and perpendicular to the (0001) layer surface through the centre of the Bragg peaks of the rare earth thin layer or yttrium seed. These scans were defined by two components, $q_z \parallel [0001]$ and $q_x \parallel [10\bar{1}0]$. Scans in which q_x were varied are referred to as transverse scans while those in which q_z varied are referred to as longitudinal

scans. The Bragg reflections are given by the 4-index, Miller–Bravais notation ($hkil$), with $i = -(h+k)$, where each of the indices is related to the q components and the lattice parameters as $h = q_x(4\pi/a\sqrt{3})^{-1}$ and $l = q_z(2\pi/c)^{-1}$. The wavevector resolution was measured using the sapphire peaks and was typically $\sim 5.0 \times 10^{-4}$ Å^{-1} in the scattering plane. The scattering was measured around the (0002), (0004), (0006), (10$\bar{1}$5) and ($\bar{1}$015) reflections of both the rare earth and yttrium layers.

2.2. Longitudinal scans

When the wavevector transfer was parallel to the [0001] growth direction, the lattice parameter in the growth direction, the thickness of the layer and the variation of the strain and roughness of the top and bottom surfaces can be obtained.

The scattering from an ideal layer consisting of $N + 1$ planes with an inter-planar spacing, c, is given by

$$I(q_z) = |F(q_z)|^2 \frac{\sin^2(Nq_zc/2)}{\sin^2(q_zc/2)}, \tag{1}$$

where $F(q_z)$ is the structure factor of the planes. This equation shows that there are strong Bragg peaks when $q_z = |\boldsymbol{q}_z| = \frac{2\pi}{c}l$, where l is a Miller index. Satellite peaks, also known as Pendellösung fringes [10], are present when $q_z = (2\pi(M + 1/2))/cN$, where M is an integer. The position of the Bragg peaks determines the average c lattice parameter and so gives a measure of the mean strain in the growth direction. The satellite positions depend on cN and allow the thickness of the layer to be determined. The width of the main Bragg peak also allows, in principle, the layer thickness to be determined. However, such an analysis is only valid if the width of the Bragg peaks is independent of the Bragg reflection, l, but in this study they have a width dependent on the index l. Babkevich *et al* [11] have summarized the effect of finite sample thickness and inhomogeneous strain on the width and shape of the Bragg peaks and the dependence of the FWHM on the index l. For a sample with a linear variation of lattice parameter, the resulting Bragg peaks have an approximately Gaussian lineshape and the FWHM varies linearly with the index l. Sufficiently high strains reduce the intensity of the main Bragg peak, broaden it and cause the disappearance of the thickness fringes. For a random, Gaussian, variation of the strain the FWHM of the Bragg peak varies quadratically with the index l. It is then possible in principle to distinguish the effect of the broadening of the Bragg reflections due to inhomogeneous strain from the broadening of Bragg reflections due to finite layer thickness, because the latter broadening is not l-dependent, whereas the former is l-dependent.

2.3. Transverse scans

The transverse scans were performed by varying the scattering vector perpendicular to the growth direction through the Bragg reflections. This allows information about the deformation of the planes parallel to the growth direction to be extracted. Flat, undistorted planes give rise to sharp Bragg-like delta function scattering. The results of this study are more complicated because the peaks are broad in q_x and display a two-component lineshape. These effects can arise in two ways. Firstly, the planes may be distorted away from their ideal position, with the distortion extending over a finite distance—the correlation length. Subsidiary peaks or two-component lineshapes can then arise if the distortions are periodic deformations, such as may be caused by a periodic array of misfit dislocations [12]. Such periodic distortions with a finite correlation length give rise to the same broadening and position in a wavevector q_x

around each Bragg reflection, l. The relative intensity of the Bragg peak components varies due to a Debye–Waller effect from the distortion of the planes and, by measuring the decrease in intensity as a function of l, a measure of the mean square displacements $\langle u_z^2 \rangle$ can be obtained.

The second effect that can give rise to broadening of the lineshape is the tilting of planes in a mosaic crystal. This can arise from the inevitable miscut of the substrate, which for the sapphire is about $\pm 0.5\%$, or from an intersecting network of dislocations. Usually both effects are present since, if a tilted component is to remain in contact with the substrate, the tilted components must be of finite size. Experimentally these two effects can be distinguished by comparing the scattering at different Bragg reflections because the broadening is independent of l for the first effect but proportional to l if it arises from tilted planes.

3. Experimental results

3.1. Holmium layers

3.1.1. Layer thickness. The nominal thickness of the layers was determined from the sample growth time using the calibrated fluxes of the atomic sources. The layer thicknesses were also determined by extrapolating the widths of the Bragg reflections and by measuring the position of the Pendellösung fringes, if they were present. Typical longitudinal scans are shown in figure 2 and the peaks were fitted using a Pearson VII function. The results showed that the peak shape was approximately Gaussian. The instrumental resolution function was estimated from the width of the sapphire $(11\bar{2}0)$ reflection and is narrow compared to the rare earth peak width. The observed peak width, Δq_z, is given by

$$\Delta q_z^2 = (\Delta q_z^L)^2 + \Delta_{\mathrm{IR}}^2, \tag{2}$$

where Δ_{IR} is the broadening due to the instrumental resolution function and Δq_z^L is the broadening due to the finite thickness of the sample and any imperfections. The resolution was measured using the sapphire reflection and was $\Delta q = 5.0 \times 10^{-4}$ Å^{-1} in the scattering plane.

The lineshape is predominantly Gaussian and if we assume that the inhomogeneous strain gives a width that varies linearly with q_z, whereas the width due to the thickness is independent of q_z, the thickness of the layer can be determined by extrapolating $(\Delta q_z^L)^2$ to $q_z = 0$ to give Δq_z^T. The layer thickness, T, is then given by [13]

$$T = -\frac{8 \ln 0.5}{\Delta q_z^T}. \tag{3}$$

As an example of this process, figure 3 shows the resolution corrected widths Δq_z^L, plotted as a function of q_z^2. The linear fit to the data gives a good description of the results. In the case of the thinner layer the line is almost a constant but for the thicker layer the slope is clearly significant, showing that the strain varies linearly through the layer.

The layer thicknesses were also determined from the position of the Pendellösung fringes, which could be observed as illustrated in figure 2(b) but are absent for the thickest layer, as shown in figure 2(a). The results of determining the layer thickness using the various different methods are presented in table 1. The final thickness is the best estimate of the weighted average of the different methods. There is good agreement between the nominal thickness and the thickness deduced from the x-ray experiments except for the two thickest samples. Possibly the growth rate changes as the thickness becomes larger than the critical thickness, as is also found for GaSb [11].

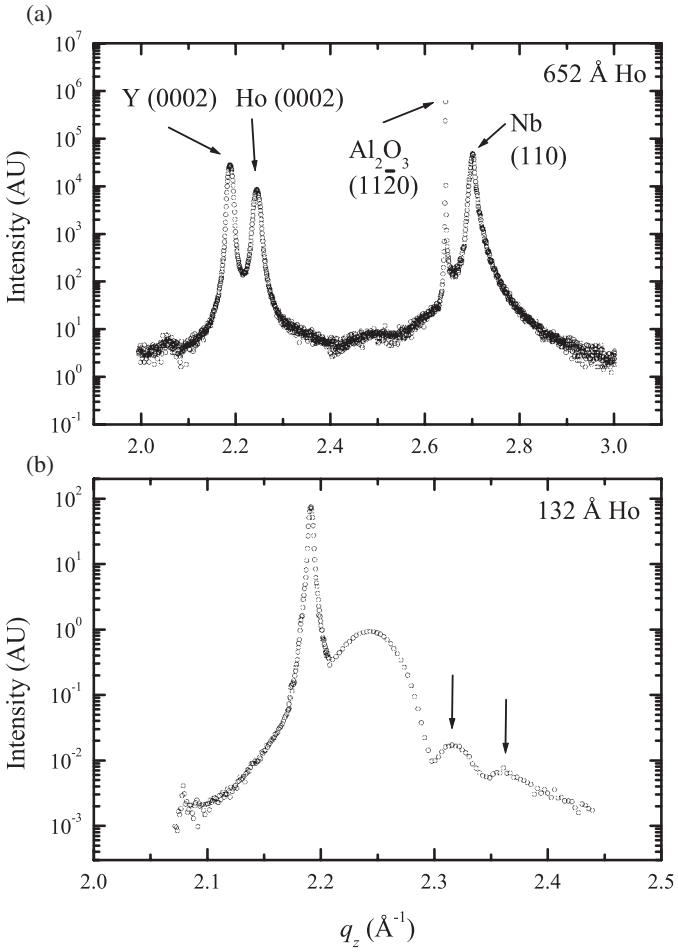

Figure 2. The scattered intensity observed when the wavevector transfer was varied longitudinally for two holmium layers. For the layer of 132 Å thickness, the Pendellösung fringes from the holmium layer are marked by arrows. The origin of the small peaks close to $q_z = 2.06$ and 2.08 are unknown.

3.1.2. Lattice parameters and strain. Bulk samples of yttrium and holmium crystallize in a hexagonal close-packed structure (HCP) with lattice constants $(a, c)_{\mathrm{Ho}} = (3.5773, 5.6158)$ Å, $(a, c)_{\mathrm{Y}} = (3.6474, 5.7306)$ Å [14]. The lattice mismatch, $f_{\mathrm{m}} = (a_{\mathrm{Ho}} - a_{\mathrm{Y}})/a_{\mathrm{Y}}$, is therefore -1.92%. The epitaxial growth of a holmium layer on yttrium results in the holmium layer being initially expanded in-plane, so the a lattice parameter is that of the yttrium substrate. This results in a compression of the out-of-plane lattice parameter, c. As the thickness of the layer increases, it becomes energetically favourable to introduce misfit dislocations to reduce the strain energy and the mean lattice parameter tends towards the bulk lattice parameter. The results obtained for the lattice parameters c_{Y}, a_{Y} and c_{Ho} are shown in figure 4. These results show that the lattice parameters of the yttrium seed are independent of the layer thickness and, for the a axis, are the same as for bulk yttrium while they are slightly larger for the c axis.

In order to minimize the systematic errors the in-plane strain, $(a_{\mathrm{Ho}} - a_{\mathrm{Y}})/a_{\mathrm{Y}}$, was measured by directly comparing the positions of the holmium and yttrium Bragg peaks and the results are shown in figure 5.

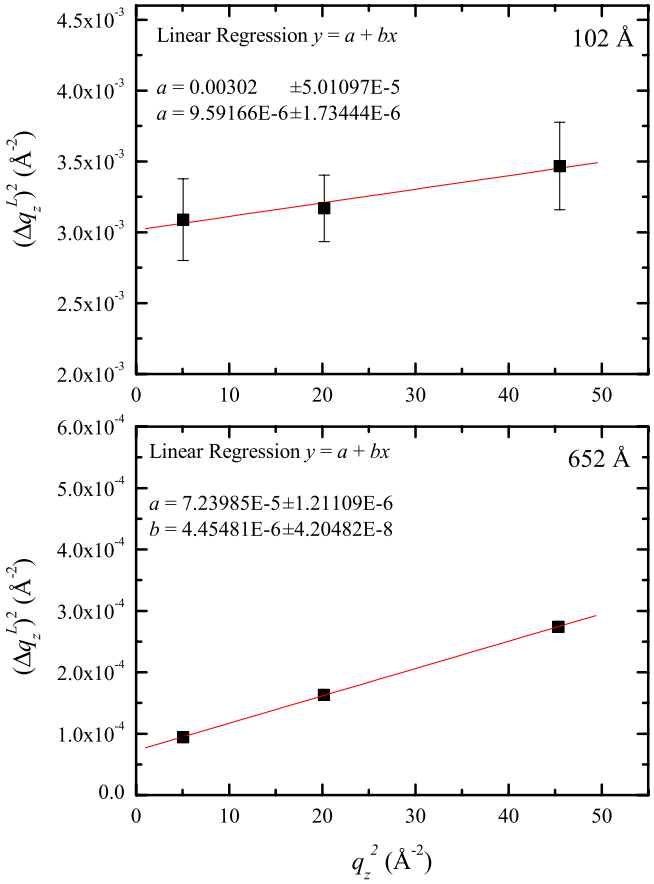

Figure 3. $(\Delta q_z^L)^2$ plotted as a function of q_z^2 for two holmium layers. The errors lie within the data points for the layer of 650 Å thickness.

The dotted curve in figure 4 shows the c lattice parameter of the holmium layer calculated from the observed in-plane strain and elasticity theory. It gives reasonable agreement with the experimentally determined values of c, whereas the lattice parameters of the yttrium seed are independent of the holmium layer thickness.

The in-plane strain, figure 5, clearly shows that there is a sharp reduction of strain in the holmium layers at a thickness of $T_c' \simeq 115(15)$ Å, while for thicker layers, the lattice constant tends towards that of bulk holmium. For layers with a thickness less than 100 Å the in-plane lattice constant of the layer is the same as that of the substrate to within 0.05%. For layers thicker than 150 Å, the in-plane lattice parameter of the layer and substrate differ significantly, showing that the relaxation of the holmium layer is about -1.1%, which is nevertheless considerably less than the -1.9% needed for full relaxation. There is little evidence of further relaxation as the thickness increases to 600 Å.

In order to clearly demonstrate the change of in-plane lattice parameters, area scans were made around the $(\bar{1}015)$ reflection for those holmium layers of thickness 49, 119 and 650 Å. These results are shown in figure 6 where the intensity has been plotted on a log scale. Lines have been added, which originate at the maximum of each peak. For the thinnest layer, the holmium and yttrium peaks are located at almost the same q_x position, indicating that the

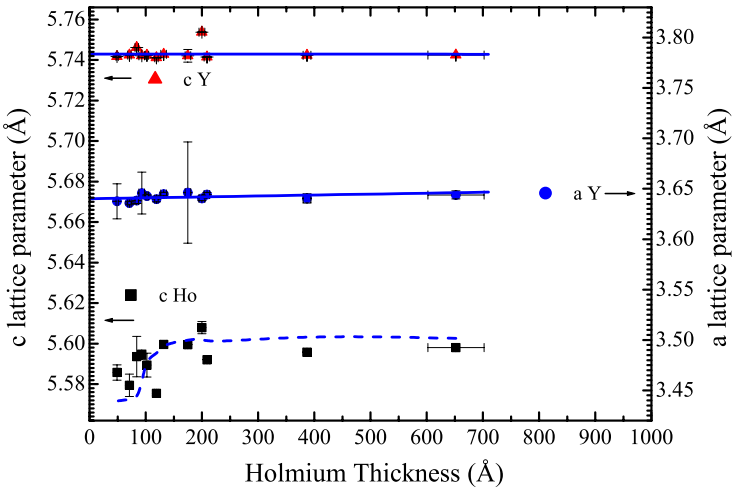

Figure 4. The lattice parameters of holmium and yttrium for the different thickness layers. The arrows next to the label show the position of the bulk lattice constant. For some points, the error bars lie within the data point.

Table 1. The thickness of the holmium layers as determined by x-ray diffraction using Pendellösung fringes and widths of the Bragg peaks using equation (2). The resulting thickness is the weighted average of the two methods and is compared to the nominal growth thickness.

Sample	Nominal thickness (Å)	Pendellösung fringe spacing (Å)	Extrapolation of Bragg peak widths (Å)	Best estimate of thickness (Å)
201	1000	—	652(50)	652(50)
201	500	415(10)	359(10)	387(7)
201	200	215(10)	208(5)	209(5)
201	100	115(5)	101(2)	102(3)
202	125	124(5)	117(4)	119(3)
202	75	74(5)	71(3)	71(3)
202	50	52(5)	47(5)	49(4)
204	180	177(5)	169(10)	175(5)
204	120	135(5)	119(10)	132(5)
204	80	90(5)	93(2)	93(5)
206	90	88(5)	83(3)	84(3)
205	200	200(5)	223(40)	200(5)

average lattice parameter of both layers is almost the same. As the thickness of the holmium layer increases, the Pendellösung fringes become more obvious, while the position of the holmium peak moves away from the yttrium peak. For the 650 Å layer the q_x separation of the peaks is clearly shown while the Pendellösung fringes are not observed.

3.1.3. Transverse scans. The scattered intensity observed when the wavevector transfer was scanned transversely through the Bragg reflections is shown in figure 7. The layer with a thickness of 71 Å displays a mostly single-component lineshape that is Gaussian in the central region. This lineshape is very similar to that observed from the yttrium seed (0002) reflection, which means that, for the thinnest layers, the micro-structure of the holmium thin

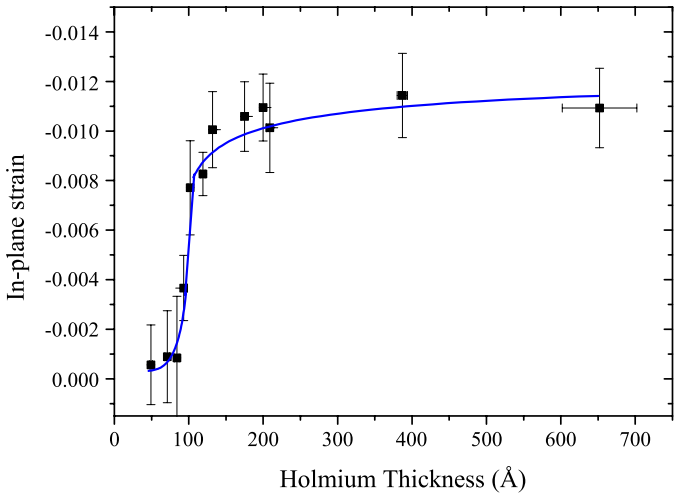

Figure 5. In-plane strain as a function of holmium layer thickness.

layer is determined by that of the yttrium seed. For thicknesses above 100 Å, there is a central sharp component that is relatively unchanged, but a diffuse component that produces a pair of symmetrical shoulders. This feature is most prominent for the layer with a thickness of 209 Å, where the diffuse component contributes about 50% to the integrated intensity. The shape of the transverse scan around the $(\bar{1}015)$ reflection also exhibited a diffuse component with a transverse width comparable to that of the (0004), but since this was much weaker than is observed for the (0002) and (0004) reflections the following analysis is restricted to the (0002) and (0004) reflections.

For the thickest samples, the lineshape is also described by a single-component Gaussian peak, but this is then substantially wider than for the corresponding yttrium reflection.

In order to analyse this effect further, the lineshapes were fitted to two Pearson VII functions. The function was first fitted to the yttrium (0002) or (0004) reflections to determine their shape. The results shown in figure 7 show that this lineshape is dominated by a single-component lineshape, with a weak secondary component. The shape of the dominant component was then held fixed for that particular reflection and represented the sharp component of the holmium reflection. A broader, diffuse Pearson VII component was also added, with no restrictions on the shape of the curve. Figure 7 shows the results of transverse scans through the holmium (0002) and (0004) reflections. The fits to the data described previously show that the width of the central sharp component varies linearly as a function of q_z. For the holmium layer with a thickness of 209 Å, the (0002) reflection had a broad component with a width of 0.014(0.005) and a shape of 2.95. This shape was common to all the broad components of the holmium (0002) reflections. The (0004) reflection had a width of 0.034(0.005) and a shape of 4.74. This shows that the broad diffuse component shows a similar q_z dependence as the narrow component. This is evidence that the holmium layer is a mosaic crystal, probably containing a network of dislocations with the Burgers vector inclined to the interface. For the thinnest holmium layer, the holmium layer grows coherently on top of each yttrium mosaic block, while for the thicker layers there is considerable further relaxation, probably because further dislocations and tilts reduce the size of the mosaic blocks in the holmium.

The results of the analysis described previously, figure 8, show that, for the thinnest layers, the integrated intensity is dominated by the sharp component whose shape and width

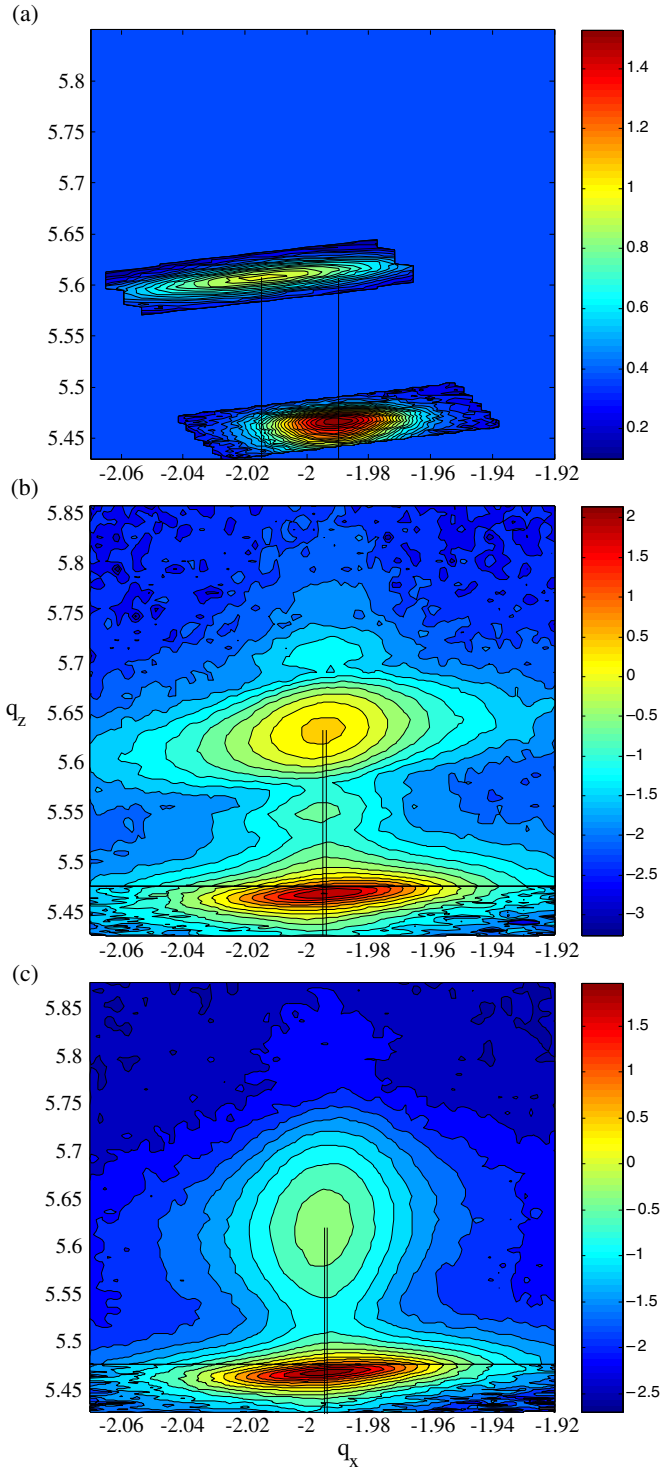

Figure 6. The scattered intensity observed when an area scan was made around the $(\bar{1}\,0\,15)$ reflection for (a) 652 Å, (b) 119 Å and (c) 49 Å layers of holmium. The intensity is plotted on a log scale and the units are $Å^{-1}$.

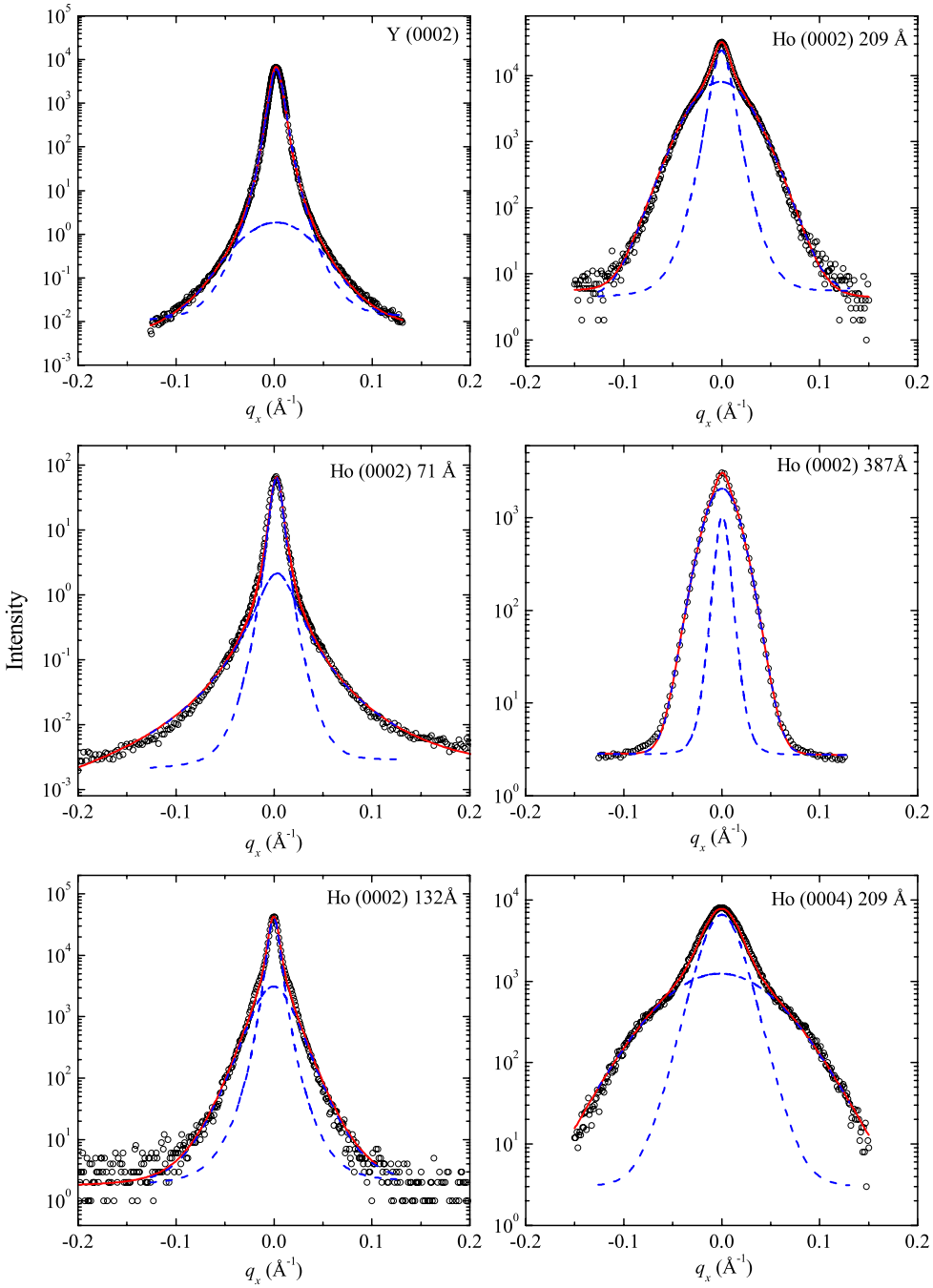

Figure 7. The scattered intensity observed when the wavevector transfer was varied transversely through the holmium and yttrium reflections for several layers' thickness. The broken curves show the two components forming the fit.

is determined by the yttrium substrate. As the layer thickness increases, this sharp component becomes less important and the scattering becomes dominated by a broader, more diffuse

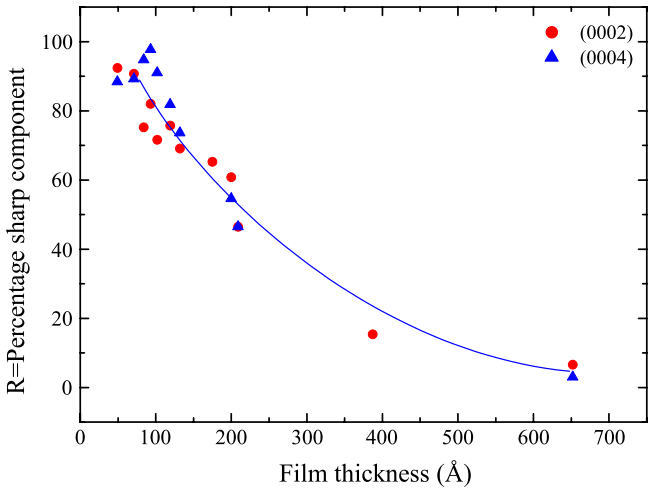

Figure 8. Percentage of the sharp component of holmium (0002) and (0004) transverse scans as a function of layer thickness.

component. For the thickest layers, this component contributes almost all of the integrated intensity.

Figure 8 also shows that the ratio R is very similar when determined from the (0002) or (0004) Bragg reflections. This suggests that there is not a large Debye–Waller factor but that the change in R with thickness is due to the extra tilting of blocks in the holmium layer.

3.2. Gadolinium layers

3.2.1. Layer thickness. Gadolinium layers were grown on a yttrium seed using similar techniques to those used for the holmium layers, with two samples grown in a terrace structure as schematically illustrated in figure 1. The sample 628A was different because the yttrium seed thickness was increased to about 10 000 Å. The layer thickness was obtained from the sample growth time using the calibrated fluxes to give the nominal thickness. In addition, the layer thickness was determined by measuring the position of the Pendellösung fringes, figure 9. The Bragg peaks were also fitted using Pearson VII functions and the results showed that the peak shapes were Gaussian. The resolution-corrected widths, Δq_z^L, of the longitudinal scans were extrapolated to $q_z = 0$ to obtain another estimate for the layer thickness.

The results of determining the layer thickness using these three methods are shown in table 2 and the final column gives the weighted average. For the 100 Å thick layer of sample SL203, the widths of the measured reflections were sufficiently broad and close to the yttrium reflection so that it was not possible to accurately determine the layer thickness from either the Pendellösung fringes or from the widths of the Bragg peaks.

3.2.2. Lattice parameters and strain. Bulk samples of yttrium and gadolinium crystallize in a hexagonal close packed structure (HCP) with lattice constants $(a, c)_{\mathrm{Gd}} = (3.6360, 5.7826)$ Å, $(a, c)_{\mathrm{Y}} = (3.6474, 5.7306)$ Å. The lattice mismatch, f_{m}, is therefore $f_{\mathrm{m}} = -0.31\%$, much smaller than in the case of Ho/Y. With a relatively small mismatch, it is necessary to analyse the theoretical strain more rigorously and include the effects of differential thermal expansion between Gd and Y, which affects the epitaxial strain, and between Gd and sapphire, which

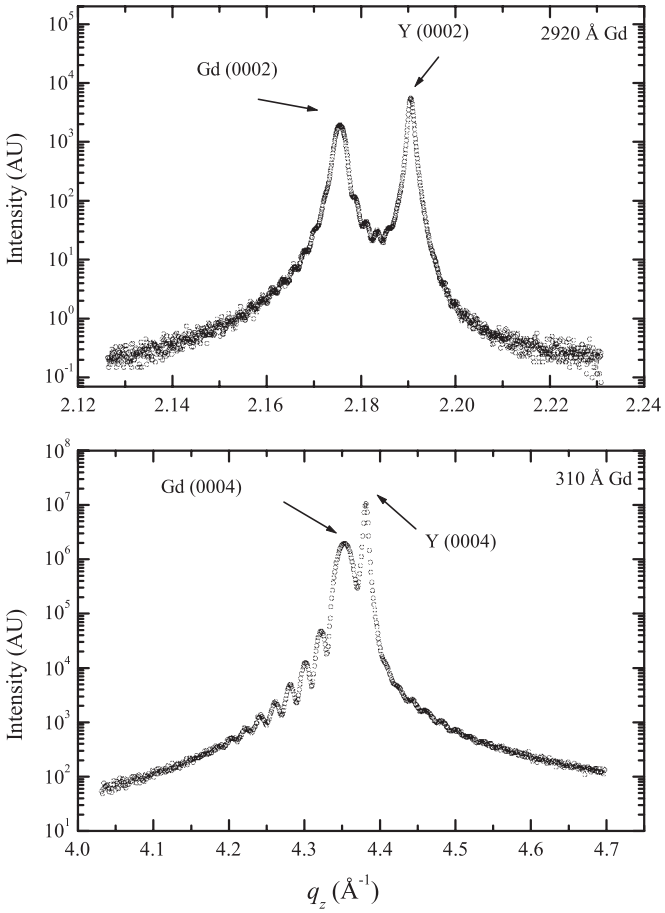

Figure 9. The scattered intensity observed when the wavevector transfer was varied longitudinally for two gadolinium layers. The Pendellösung fringes are visible for both layers.

Table 2. The thickness of the gadolinium thin layers as determined by x-ray diffraction using Pendellösung fringes and the widths of the Bragg peaks using equation (2). The resulting thickness is the weighted average of the two methods and is compared with the nominal growth thickness.

Sample	Nominal thickness (Å)	Pendellösung fringe spacing (Å)	Extrapolation of Bragg peak widths (Å)	Best estimate of thickness (Å)
203	500	517(25)	482(50)	510(25)
203	300	323(20)	278(35)	310(20)
203	200	130(15)	191(25)	170(20)
203	100	—	—	—
628A	3000	2820(150)	2950(90)	2920(75)

determines the additional strain component imposed by substrate clamping. Using values for the coefficients of thermal expansion listed by Beaudry and Gschneidner [15], the lattice mismatch at the growth temperature of 350 °C for Gd/Y is only −0.19%. This calculation assumes that the Y layer is itself unstrained at the growth temperature; in fact, there is likely to

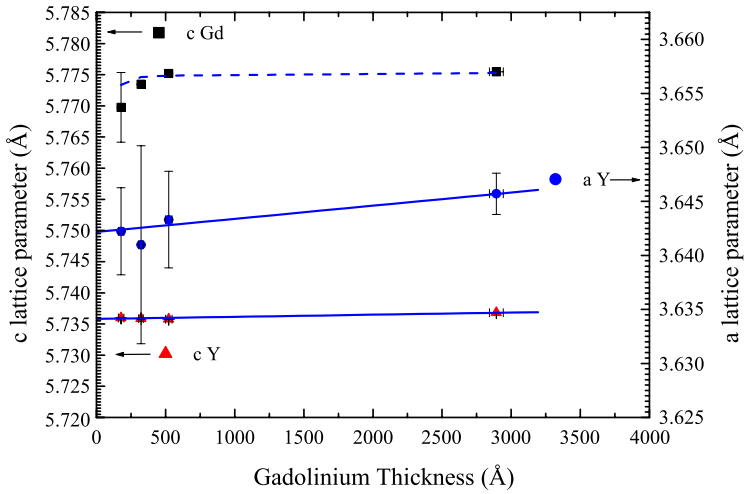

Figure 10. The lattice parameters as a function of gadolinium thickness. The arrows next to the label show the position of the bulk lattice constant.

be some compressive strain remaining from the epitaxial growth of the Y layer on the Nb buffer. This would further reduce the Gd/Y mismatch, so we may regard −0.19% as a maximum value. During cooling to room temperature after growth it is assumed that the epitaxial layers are clamped to the substrate, i.e. their in-plane thermal contraction is precisely that of sapphire. The clamping strain component in the Gd is calculated to be ≈0.1% (tensile) in our case.

The out-of-plane lattice parameters, c, and in-plane lattice parameters, a, were determined from the position of the (0002), (0004), (0006) and $(\bar{1}015)$ reflections for the yttrium seed and holmium layers and are shown in figure 10.

The a and c lattice parameters for yttrium remain relatively constant for all the layers and are consistent with a small residual compressive strain, as discussed above. There is possibly a small decrease in the c lattice parameter for the thinnest Gd layers. Note that the in-plane strain relative to the Y substrate (figure 11) is a measurement of the epitaxial strain component only.

The dotted line in figure 10 shows the expected c lattice constant calculated from the observed change in the a lattice constant. This shows a small decrease in the c lattice constant. Once again, in order to minimize systematic errors the in-plane strain relative to the yttrium substrate was determined as $(a_{\mathrm{Gd}} - a_{\mathrm{Y}})/a_{\mathrm{Y}}$. The results are shown in figure 11. The strain relative to the yttrium layer possibly shows a small decrease, similar to the holmium case, but this is inconclusive because all the points lie, within error, at a constant strain. The strain was studied further by measuring contour plots of the observed intensity around the $(0\bar{1}15)$ Bragg reflections. The results are shown in figure 12, with the intensity plotted on a log scale. For the thinnest gadolinium layer, 100 Å in thickness, the gadolinium peak is not well separated from the yttrium peak in the out-of-plane direction. Layers with a gadolinium thickness of 170 and 510 Å show a small difference in gadolinium and yttrium peak positions, which is consistent with the results of measuring the peak positions directly, and with the contraction of the gadolinium c lattice constant.

3.2.3. Transverse scans. Transverse scans were made by varying the q_x component of the scattering vector through the (0004) and (0006) Bragg reflections of the gadolinium and yttrium and the results are shown in figure 13. The results for the yttrium (0002) and (0004) transverse

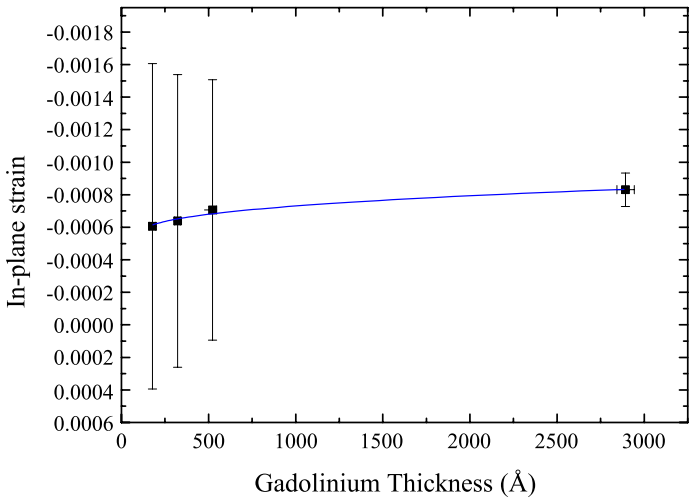

Figure 11. In-plane strain as a function of gadolinium thickness.

scans show that the yttrium layer is a mosaic crystal and the lineshape could be fitted with two Pearson VII functions. Except for the thickest 2920 Å gadolinium layer, the lineshape of the gadolinium layers could not satisfactorily be fitted with a single Pearson VII function, and so they have been fitted to two Pearson VII functions and a linear background. Both components are shown (broken curves), with the sum shown as the full curve. For the 170 Å thick layer of gadolinium, the lineshape is essentially the same as that of the yttrium lineshape, showing that the structure of the layer is determined by the yttrium layer.

For the 2920 Å thick gadolinium layer, the transverse lineshape is a single component.

3.3. Scattering from dislocations and discussion

The structure of holmium thin layers on yttrium can be understood as the result of the introduction of dislocations into a thin layer. Similar behaviour has also been observed in epitaxial semiconductor GaSb/InAs thin layers [11].

The scattering profile of a single dislocation (small dislocation densities) can be calculated by using the theory of elasticity to calculate the atomic displacements from the undistorted crystal [16] and the results for the scattering from an edge dislocation are shown in figure 14. The results of modelling the scattering show that there is a central Bragg-like component, whose width is independent of q_z and determined by the width assumed for the sample. This component is a result of the scattering from largely undistorted regions of the crystal. There are also symmetrical shoulders either side of this Bragg-like component, whose position vary linearly as a function of q_z and arises from the tilted planes near the core of the dislocation.

The experimental results described previously show that all the holmium thin layers with a thickness less than 652 Å displayed Pendellösung fringes with the broadening of transverse scans that is normally consistent with a mosaic crystal. However, the presence of Pendellösung fringes means it is unlikely that those holmium layers thinner than 652 Å had a network of dislocations with the Burgers vector inclined to the interface, because the presence of these types of dislocations has been shown to give inhomogeneous strains that destroy the Pendellösung fringes. This points to the following model. For thin holmium layers (<115 Å) the layer is lattice matched to the yttrium substrate with $R \sim 0.05\%$. There are then few,

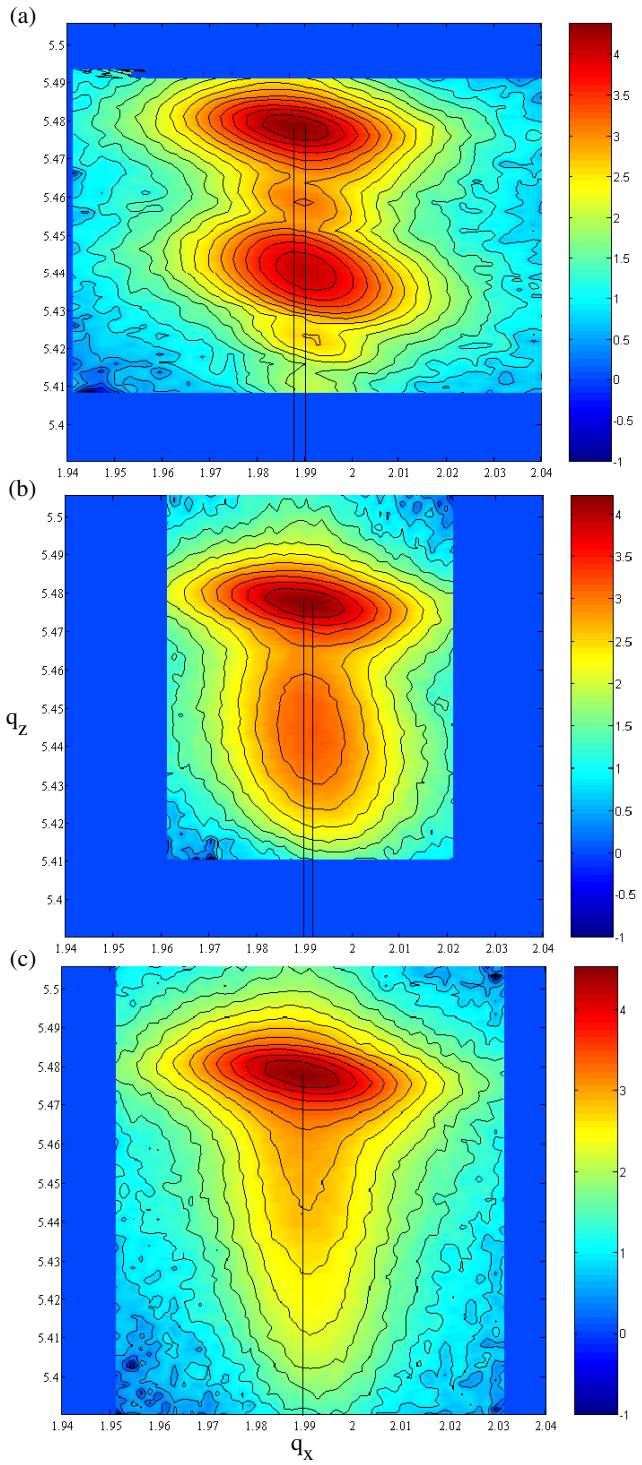

Figure 12. The scattered intensity observed when a contour plot was made around the $(0\bar{1}15)$ reflection for (a) 510 Å, (b) 170 Å and (c) 100 Å layers of gadolinium. The intensity is plotted on a log scale and the units are $Å^{-1}$.

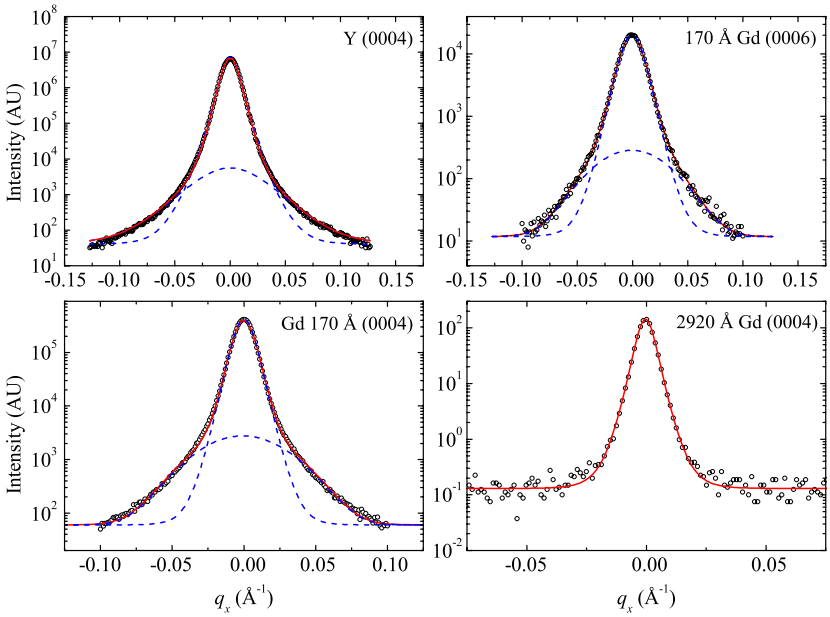

Figure 13. Transverse lineshape of various gadolinium and yttrium reflections for different layer thicknesses. The broken curves show the two components forming the fit.

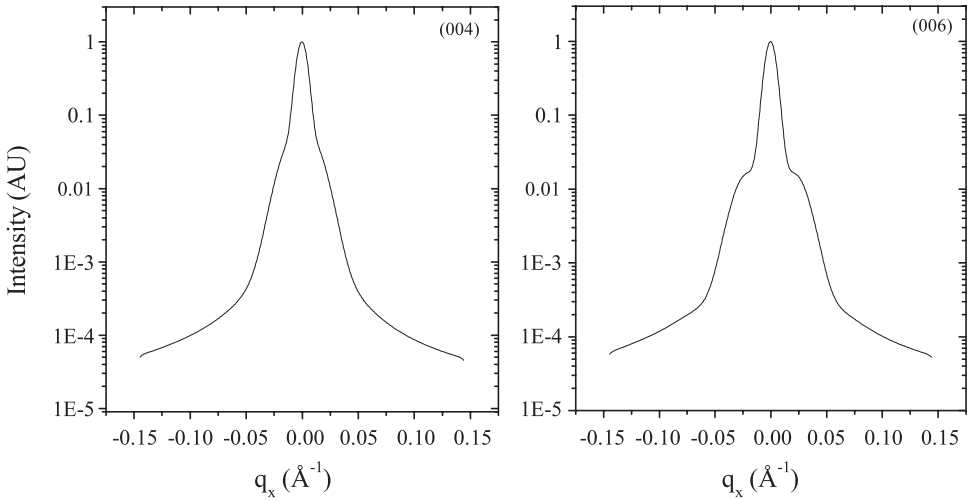

Figure 14. The simulated scattering form an isolated edge dislocation for 36 monolayers, with a transverse width of 1001 atoms and Burgers vector $|b| = a$, where a is the lattice constant. The profile has been 'smoothed' by convolution with a Pearson VII amplitude.

if any, dislocations arising from the lattice strain. For thicker layers the lattice relaxes with $R \sim 1.1\%$ and the intensity of the broad component in the transverse scan increases while the Pendellösung fringes persist. This is consistent with the introduction of edge dislocations at or near the interface to reduce the strain. These edge dislocations with a mean spacing of about 300 Å are probably randomly pinned by the mosaic domain structure of the yttrium

substrate, because we do not observe satellite peaks from a regular dislocation structure. The presence of edge dislocations at the interface does not destroy the Pendellösung fringes in the semiconductor systems [13].

Using the continuum theory of Matthews and Blakeslee [1] the critical thickness T_c for the introduction of misfit dislocations can be calculated assuming the Burgers vector, slip system and the core parameter $\rho_c = 2$ are known. The critical thickness for an edge dislocation with a Burgers vector of $\boldsymbol{b} = 1/3\langle 11\bar{2}0\rangle$, in conjunction with the {0001} slip plane, is $T_c = 11$ Å for holmium on yttrium and 116 Å for gadolinium on yttrium. For dislocations with the Burgers vector inclined to the interface, the critical thickness is expected to be larger. For holmium on yttrium, the value of the critical thickness for edge dislocations is about one-tenth of the observed critical thickness $T_c' \simeq 115$ Å. The functional form of the expression for T_c makes it unlikely that the calculated critical thickness can be in error by greater than a factor of two, say. Presumably the reason for this discrepancy is the difficulty of nucleating the dislocations, as discussed by Jain *et al* [17]. Our results suggest that the creation of the edge dislocations is inhibited until the thickness is about 114 Å and there is then a rapid increase in the number of edge dislocations presumably at the interface between the holmium and yttrium layers. These dislocations do not, however, release all the strain and with increasing thickness the residual strain is possibly slowly relaxed by the introduction of a network of dislocations with components of the Burgers vector perpendicular to the growth plane. This gives rise to inhomogeneous strain in the layer and to the disappearance of the Pendellösung fringes.

In the case of gadolinium on yttrium there was little change in the strain of the layer, no obvious change in the lineshape of the transverse scans and the Pendellösung fringes were also present for all layer thicknesses. The yttrium layer showed transverse broadening as a function of q_z which is characteristic of a mosaic crystal, as well as the absence of Pendellösung fringes, showing that this layer contained a network of dislocations, some of which had a Burgers vector inclined to the interface.

The observation of Pendellösung fringes in layers as thick as the 2920 Å thick layer of gadolinium is unusual. It is possibly a consequence of the unusually thick 10 000 Å seed layer. It is known [4] that the width of the transverse scans in thick layers tends to decrease with increasing thickness.

Presumably the top surface of a thick layer may be relatively free of dislocations with an inclined Burgers vector because the dislocations lower down in the layer have relaxed the strain between the yttrium and niobium so there is no strain energy at the top of the layer to produce dislocations by glide or climb. This would give a relatively dislocation-free surface on which the gadolinium grows. Because of the low mismatch (-0.31%) between the gadolinium and yttrium, the gadolinium layer then grows epitaxially and coherently strained (pseudomorphically), without the introduction of dislocations. The small measured strain (0.06%) corresponds to an edge dislocation spacing of 6000 Å, much larger than the yttrium mosaic domain size. The strain may therefore arise from the strain of the gadolinium within each domain. The misfit strain for gadolinium and yttrium, -0.31%, is smaller than the strain remaining in the holmium layers when $T > T_c'$. The results for both materials then suggest that edge dislocations cannot be nucleated to release all of the strain, as suggested by the Matthews and Blakeslee theory.

4. Summary

The scattering from the yttrium substrate showed that the width of the Bragg peaks are proportional to q_z, as expected for a mosaic crystal. The thinnest holmium layers grow pseudomorphically on the yttrium seed and transverse scans through the Bragg peaks give

a single-component lineshape that is similar in shape to the yttrium peak lineshape. Above a thickness of 115 Å the strain in the holmium layer is released by the introduction of randomly situated edge dislocations. The transverse lineshape has two components and is consistent with the scattering expected from a sample after the introduction of edge dislocations. For the thickest 652 Å thin layer, the transverse lineshape reverts to a single-component lineshape that is wider than the seed layer lineshape and is consistent with the scattering from a mosaic crystal. The measurements of the lattice parameters of holmium and yttrium show that there is a sudden relaxation of the in-plane strain at $T_c' \simeq 115(15)$ Å. Calculations of the critical thickness using the continuum theory of Matthews and Blakeslee give a critical thickness of $T_c = 11$ Å for edge dislocations. The discrepancy of T_c and T_c' is probably due to the problem of nucleation of dislocations in the holmium layer.

For the gadolinium layers grown on yttrium, measurements of the lattice constants showed there was no large change of the in-plane strain. The transverse lineshape remained largely unchanged for all the gadolinium thin layers and was similar to that of the yttrium seed. The gadolinium layer remains lattice-matched to the yttrium substrate to better than 0.01% and grows pseudomorphically even for the thickest 2920 Å layer.

The holmium on yttrium and gadolinium on yttrium therefore present different results that are a direct result of the different lattice mismatches for these two systems. Both systems show that the difficulty of nucleating dislocations inhibits the relaxation of lattice parameters as predicted by simple theories.

Acknowledgments

This work was funded by the UK Engineering and Physical Sciences Research Council (EPSRC). The work was performed on the EPSRC-funded XMaS beamline at the ESRF and we are grateful to the beamline team for their expertise. We would also like to thank A Yu Babkevich for help with these experiments and useful discussions.

References

[1] Matthews J W and Blakeslee A E 1974 Defects in epitaxial multilayers *J. Cryst. Growth* **27** 118–25
[2] Downes J R, Dunstan D J and Faux D A 1997 Analysis of the shortcomings of the Matthews–Blakeslee theory of critical thickness at higher strains *Phil. Mag. Lett.* **76** 77–81
[3] McMorrow D F, Cowley R A, Gibaud A, Ward R C C and Wells M R 1993 Structure of niobium thin films on sapphire *Appl. Phys. Lett.* **63** 2195–7
[4] Wildes A R, Cowley R A, Ward R C C, Wells M R, Jansen C, Wireen L and Hill J P 1998 The structure of epitaxially grown thin films: a study of niobium on sapphire *J. Phys.: Condens. Matter* **10** L631–7
[5] Grier E J, Jenkins M L, Petford-Long A K, Ward R C C and Wells M R 2000 Misfit dislocations of epitaxial (110) niobium ‖ (110) sapphire interfaces grown by molecular beam epitaxy *Thin Solid Films* **358** 94–8
[6] Barabash R I, Donner W and Dosch H 2001 X-ray scattering from misfit dislocations in heteroepitaxial film: the case of Nb(110) on Al_2O_3 *Appl. Phys. Lett.* **78** 443–5
[7] Cowley R A and Wildes A R 2003 Structure of yttrium films on niobium, unpublished
[8] Grier E 2000 Microstructural characterisation of epitaxial rare earth metal based films *PhD Thesis* University of Oxford
[9] Hirth J P and Lothe J 1982 *Theory of Dislocations* 2nd edn (New York: Wiley)
[10] Azaroff L V, Kaplow R, Kato N, Weiss R J, Wilson A J C and Young R A 1974 *X-ray Diffraction* (*International Series in Pure and Applied Physics*) (New York: McGraw Hill)
[11] Babkevich A Yu, Cowley R A, Mason N J, Sandiford S and Stunault A 2002 X-ray scattering from epitaxial GaSb/InAs thin films below and above the critical thickness *J. Phys.: Condens. Matter* **14** 7101–21
[12] Babkevich A Yu, Cowley R A, Mason N J and Stunault A 2000 X-ray scattering, dislocations and orthorhombic GaSb *J. Phys.: Condens. Matter* 4747–56

[13] Babkevich A Yu, Cowley R A, Mason N J and Weller S 2002 X-ray scattering from dislocation arrays in GaSb *J. Phys.: Condens. Matter* **14** 13505–28
[14] Wyckoff R W G 1965 *Crystal Structures* (New York: Interscience)
[15] Gschneidner K A Jr and Beaudry B J 1978 *Handbook of the Physics and Chemistry of Rare Earths* vol 1 (Amsterdam: North-Holland)
[16] Landau L D and Lifshitz E M 1979 *Theory of Elasticity* (*Course of Theoretical Physics* vol 7) (Oxford: Pergamon)
[17] Jain S C, Harker A H and Cowley R A 1997 Misfit strain and misfit dislocations in lattice mismatched epitaxial layers and other systems *Phil. Mag.* A **75** 1461–515